

# We are IntechOpen, the world's leading publisher of Open Access books Built by scientists, for scientists

6,300

Open access books available

170,000

International authors and editors

185M

Downloads

Our authors are among the

154

Countries delivered to

TOP 1%

most cited scientists

12.2%

Contributors from top 500 universities



WEB OF SCIENCE™

Selection of our books indexed in the Book Citation Index  
in Web of Science™ Core Collection (BKCI)

Interested in publishing with us?  
Contact [book.department@intechopen.com](mailto:book.department@intechopen.com)

Numbers displayed above are based on latest data collected.  
For more information visit [www.intechopen.com](http://www.intechopen.com)



# Model of an Artificial Blastula for Assessing Development Toxicity

*František Muzika and Jerzy Górecki*

## Abstract

We are concerned with computer simulations of a ring of 20 coupled CSTRs with glycolytic oscillatory reaction. Each CSTR represents an artificial cell, and the ring can be regarded as an artificial blastula. The cells are coupled to two adjacent CSTRs via the mass exchange of reagents. The glycolytic oscillatory reaction is simulated using the two-variable core model. Our work is focused on the classification of stationary discrete nonuniform concentration patterns (discrete Turing patterns). The control parameters in simulations are autocatalytic and inhibition rate coefficients, as well as the transport rate coefficients. We performed the analysis of stability and bifurcations of stationary states to identify the stationary states. The inflow of reagents into each CSTR was used to initiate a particular pattern. We propose a method to assess the morphogenetic toxicity of any chemical from a database by switching between patterns or between patterns and oscillations. Moreover, we investigated nonuniform patterns that create discrete concentration waves inside the ring of 20 coupled cells, which can trigger gastrulation.

**Keywords:** discrete turing patterns, glycolysis, 2D artificial blastula, cheminformatics, morphogenesis toxicity

## 1. Introduction

Cheminformatics tools allow us to define information and parameters of various chemicals influencing more complex systems. The information and parameters are focused on chemical structure, experimental and physicochemical data, and toxicity. The toxicity data can concern living tissues, metabolic pathways [1], DNA [2, 3], RNA, [4, 5], gut microbia [6], or mitochondrial toxicity [7]. Cheminformatics is also essential for the development of new drugs [8–11] and for the assessment of their toxicity [12]. Since the databases of chemicals are extensive and count in millions of elements, the approach of using artificial intelligence [13], artificial neural networks [14], and machine learning seems to be the only method to deal with such a huge amount of collected information [15].

In this paper, we are concerned with the toxicity of chemicals causing morphogenetic malfunctions. The malfunctions can be seen as deformed organs, excessive or missing limbs, and fingers. The toxic factors can also terminate morphogenesis, causing the death of living organisms. On the other hand, the identification of toxic factors

can be useful for slowing down the growth of cancer cell clusters. As an alternative to experiments with actual living cells, we created the 2D model of an artificial blastula, which mimics a multicellular living organism in its developmental stage (blastula). Within our model, toxicity and morphogenic malfunctions can be recorded as the formation and destruction of discrete nonuniform patterns and switching between them. These patterns were first introduced by A. Turing in his pioneering study [16]. They are partially responsible for yeast budding [17] and are expected to play a key role during fetal development and gastrulation [18], limb development [19], and fingers development [20]. While the stationary Turing pattern can occur under conditions of faster transport rate of inhibitor species, usually under the scheme “short-range activation and long-range inhibition” [21, 22], they can also occur for equal transport rates of both activator and inhibitor, provided that the overall kinetics is enhanced, and the system is properly perturbed [23–26]. Turing patterns have been proven experimentally [27–32], but for its occurrence, the activator molecule transport rate has to be slowed down by different agents. The occurrence of discrete Turing patterns has been shown experimentally and in models in various artificial systems using the Belousov-Zhabotinsky reaction and its modifications [33–38].

Our recent research shows it is possible to make transitions between uniform oscillations and discrete nonuniform patterns [39]. This can be used for chemical computing as well as a type of chemical memory. Moreover, nonuniform patterns can also be used as the output of chemical classification. The network considered in this paper can be used as a classifier under different kinetic and transport parameters and under different network topology. The reaction parameters and coupling constants have to be optimized for each topology. Evolutionary algorithms are frequently used for parameter optimization. Once optimized, even a small network can classify schizophrenia [40] or color of points on the Japanese flag [41] with accuracy exceeding 90%.

In this chapter, we would like to show how the 2D blastula model can exhibit various discrete nonuniform patterns and how these patterns can be quenched by varying kinetic parameters, transport parameters, and the inflow of the substrate.

## 2. Methods

### 2.1 Theoretical setup

To model a small multicellular organism of unspecialized cells having only one layer of cells, a blastula, we chose a ring of  $N = 20$  equivalent cells representing the cross section of a blastula. This theoretical setup, see **Figure 1**, follows the morphogenesis work of A. Turing [16]. The only difference in our case is that both activator and inhibitor are transported at the same rate, as proposed in work by Vastano et al. [23, 24]. Under such circumstances, both nonuniform patterns and uniform oscillations exist simultaneously. If initially, all cells are in the same state, uniform, fully synchronized oscillations appear. In order to obtain a nonuniform stationary pattern, the initial state should be nonhomogeneous. Alternatively, a nonuniform stationary pattern can be obtained by a nonhomogeneous perturbation of synchronized oscillations. This is schematically shown in **Figure 1**, where in **Figure 1a**) the 2D blastula model operates in a regime of uniform oscillations, and it acts as 20 synchronized cells. After it is perturbed, it goes into a regime of a discrete nonuniform pattern (discrete Turing pattern) (see **Figure 1b**). Afterward, it can be switched into other discrete

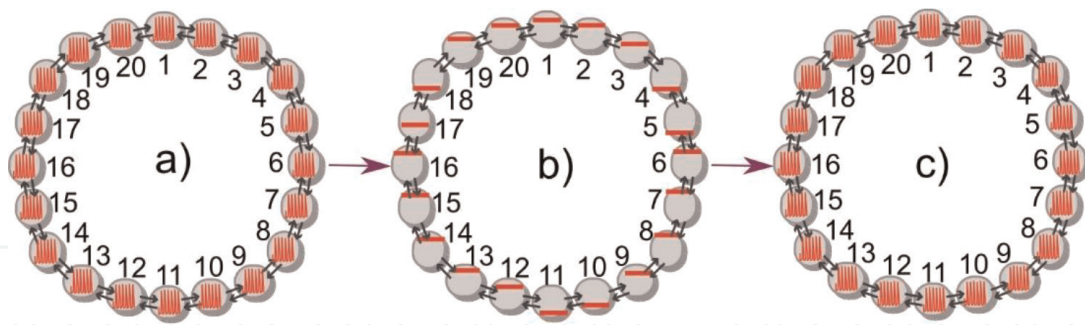


**Figure 1.**  
 The array of  $N = 20$  coupled cells taken as a 2D blastula model: a) regime of uniform oscillations, b) regime of discrete nonuniform patterns, and c) regime of uniform oscillations again. Black arrows represent the reagent exchange between cells. Each cell is numbered. Blue arrows represent perturbation leading to a transition to discrete nonuniform pattern from uniform oscillations and vice versa. The applied perturbation is shown in **Figure 3**.

nonuniform patterns (see Results) by an additional perturbation, or it can be switched back to uniform oscillations, as shown in **Figure 1c**.

## 2.2 Model of glycolysis

Our 2D blastula model consists of 20 coupled cells in which chemical reactions occur. A separated cell can be modeled using the kinetic equation:

$$\frac{dZ}{dt} = F(Z, P), \quad (1)$$

where vector  $Z = (x_1, \dots, x_m)$  represents concentrations of reagents involved and vector  $P = (p_1, \dots, p_l)$  represents the values of  $l$  parameters that influence the reaction rates. The vector function  $F(Z, P) = (F_1(Z, P), \dots, F_m(Z, P))$  represents the reaction rates. For  $N$  coupled cells in a ring geometry communicating via diffusive transport, the system of evolution equations is

$$\left(\frac{dZ}{dt}\right)_i = Q_i(Z_i, P) = F(Z_i, P) + \text{diag}(K_d)(Z_{i+1} - 2Z_i + Z_{i-1}), i = 1, \dots, N, \quad (2)$$

and the boundary condition is  $Z_i = Z_{i+N}$ . Vector  $K_d = (k_1, \dots, k_m)$  represents a vector of the transport rate coefficient for each species.

In the case considered in our study, all species have the same transport rate coefficient in between all cells, and thus  $k_d = k_1 = k_2 = \dots = k_m$ . To describe reaction kinetics, we apply the core model of glycolysis [42] on Eq. (2), yielding to equations:

$$\begin{aligned} F(x_i, y_i, P) &= \nu_i(t) + \sigma_{inh} \frac{y_i^n}{M^n + y_i^n} - \sigma_M \frac{x_i(1+x_i)(1+y_i)^2}{L + (1+x_i)^2(1+y_i)^2} \\ F(y_i, y_i, P) &= \phi \sigma_M \frac{x_i(1+x_i)(1+y_i)^2}{L + (1+x_i)^2(1+y_i)^2} - k_{sy_i} - \phi \sigma_{inh} \frac{y_i^n}{M^n + y_i^n} \end{aligned} \quad (3)$$

$$i = 1, \dots, N,$$

where  $x_i$  and  $y_i$  represent ATP and ADP concentration in the  $i$ -th cell, respectively. The function  $\nu_i(t)$  describes the ATP inflow rate,  $\phi$  if the ratio of dissociation

constants of ATP to ADP,  $n$  is Hill coefficient,  $L$  is allosteric constant,  $k_s$  is coefficient of degradation of ADP,  $M$  is Michaelis constant,  $\sigma_M$  is autocatalytic rate coefficient, and finally  $\sigma_{inh}$  is inhibition rate coefficient. In simulations, we used the values of parameters proposed by Moran and Goldbeter [42]  $n = 4$ ,  $L = 10^6$ ,  $k_s = 0.06 \text{ s}^{-1}$ ,  $\phi = 1$ . The values of other parameters determining reaction kinetics,  $\sigma_{inh}$ ,  $k_d$ , and  $\nu_i(t)$ , were modified in our simulations. The value of  $\sigma_M = 100 \text{ s}^{-1}$  was used in all simulations.

### 2.3 Varying parameters to set up the 2D blastula model

Our 2D blastula model has to have carefully chosen parameters, so it can exhibit the coexistence of discrete patterns and nonuniform oscillations. The core model of glycolysis for one cell shows uniform oscillations, stable uniform stationary state, birhythmicity, and hard excitation [42] under fixed autocatalytic rate coefficient  $\sigma_M = 10 \text{ s}^{-1}$ , varied inhibition rate coefficient  $\sigma_{inh} \in [0 \text{ s}^{-1}, 4 \text{ s}^{-1}]$ , and varied ATP inflow rate  $\nu \in [0 \text{ s}^{-1}, 2 \text{ s}^{-1}]$ . Since we created a model of arrays of coupled cells with the core model of glycolysis, we had to add transport in between cells originally described by  $k_{ATP}$  as the transport rate coefficient for ATP and  $k_{ADP}$  as the transport rate coefficient of ADP. Further studies showed if we increase  $\sigma_M > 80 \text{ s}^{-1}$ , we can have an equal transport rate coefficient  $k_d$  for both ATP and ADP. The increment of  $\sigma_M$  and  $\sigma_{inh}$  can be realized experimentally by increasing temperature [43], increasing pH, by the addition of hydrocarbonates [44], or addition of other metabolites [45]. The value of  $k_d \in [300; 6000] \text{ s}^{-1}$  for whole cellular surface [46]. For intercellular communication, only part of the surface is used.

### 2.4 Solution diagram

For the analysis of stability and location of bifurcations of stationary states and for simulations of the system, we used the program CONT [47, 48]. A solution diagram was obtained as the result of a one-parameter continuation. The solution diagram for ADP concentration in the first cell as a function of  $\sigma_{inh}$  and fixed  $\sigma_M = 100 \text{ s}^{-1}$ ,  $k_d = 0.1 \text{ s}^{-1}$  is shown in **Figure 2**. The system has a stable uniform stationary state from  $\sigma_{inh} \in [0 \text{ s}^{-1}, 17.8 \text{ s}^{-1}]$  and  $\sigma_{inh} \in [95.3 \text{ s}^{-1}, 100 \text{ s}^{-1}]$  marked by a solid red line. In between the stable uniform stationary state, there is a region of stable uniform oscillations that occurred via subcritical Hopf bifurcation from the left side and supercritical Hopf bifurcation from the right side, shown by black curves of minima and maxima of concentration of ADP. Inside this region of stable uniform oscillations, there are multiple branches of discrete Turing patterns that occurred from branch point bifurcations marked by a blue dashed line. These patterns are secondarily stabilized by supercritical Hopf bifurcations and, therefore, they cannot occur spontaneously just by varying  $\sigma_{inh}$  or  $k_d$ . The stable discrete nonuniform patterns are marked by solid red curves. The solution diagram only shows possibilities of stationary concentrations of ADP in the first cell. All discrete nonuniform patterns shown simultaneously in all 20 cells are discussed in the Results section.

## 3. Results

Our goal is to provide a method for assessing organism development toxicity. To create the method, we need to map all possible patterns inside the 2D blastula model.



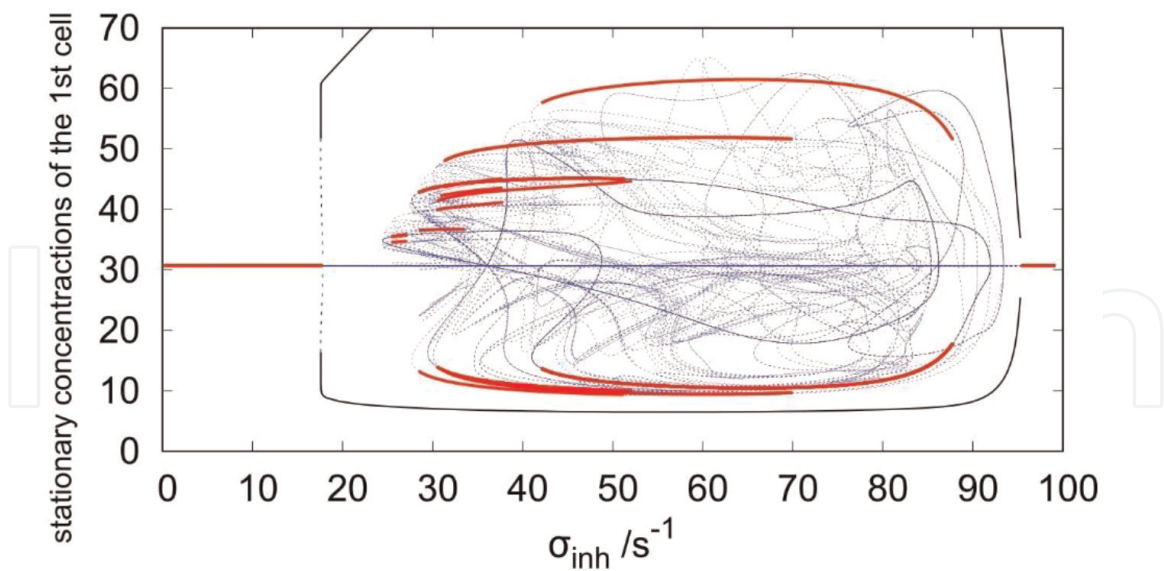


**Figure 2.** Solution diagram of ADP in the first cell for  $\sigma_M = 100 \text{ s}^{-1}$ ,  $k_d = 0.1 \text{ s}^{-1}$ ,  $\nu = 1.84 \text{ s}^{-1}$ . Red solid curve – Stable stationary state, blue dashed curve – Unstable stationary state, solid black curve – Stable minima and maxima of glycolytic oscillations, dashed black curve – Unstable minima and maxima of glycolytic oscillations, Hopf bifurcation points, and branch points are omitted for the purpose of readability of the solution diagram.

Letter	Range of stationary concentration of ADP
A	[1, 12]
B	(12, 28)
C	[28, 36]
D	(36, 47)
E	[47, 100]

**Table 1.** Assignment of a letter to a stationary concentration of ADP.

For the purpose of machine reading and loading the resulting discrete patterns, we are assigning a letter to certain ranges of stationary concentrations of ADP, **Table 1**.

A uniform stationary state has thus pattern C<sup>20</sup> with its dimensionless stationary concentration of ADP = 30.6667.

The 2D blastula model can operate in a regime of uniform oscillations, uniform stationary state, and according to **Figure 2** at least 12 discrete nonuniform patterns are possible for  $k_d = 0.1 \text{ s}^{-1}$ . The analysis of the occurrence of the discrete nonuniform patterns was done by varying the input concentration of ATP by trying all the values within range  $\nu_i(t) \in [0 \text{ s}^{-1}, 4 \text{ s}^{-1}]$  for each cell and also for all combinations of 20 cells.

The same analysis can be done for any chemical input we define as a metabolic pathway inside each cell. The guide for our analysis under constant  $k_d$  is the solution diagram in **Figure 2**, or it could be a bifurcation diagram in the whole parameter plane of  $k_d$  and  $\sigma_{inh}$ . A simulation of a transition between uniform oscillations and discrete nonuniform patterns on six randomly chosen cells is shown in **Figure 3**. The figure is divided into four subfigures illustrating the perturbations and concentrations in the time interval [0 s, 4000 s]. **Figure 3a**) shows the values of  $\nu_1(t)$ ,  $\nu_6(t)$ , and  $\nu_{11}(t)$ . **Figure 3b**) shows the values of  $\nu_2(t)$ ,  $\nu_{10}(t)$ , and  $\nu_{20}(t)$ . **Figure 3c**) shows the time-

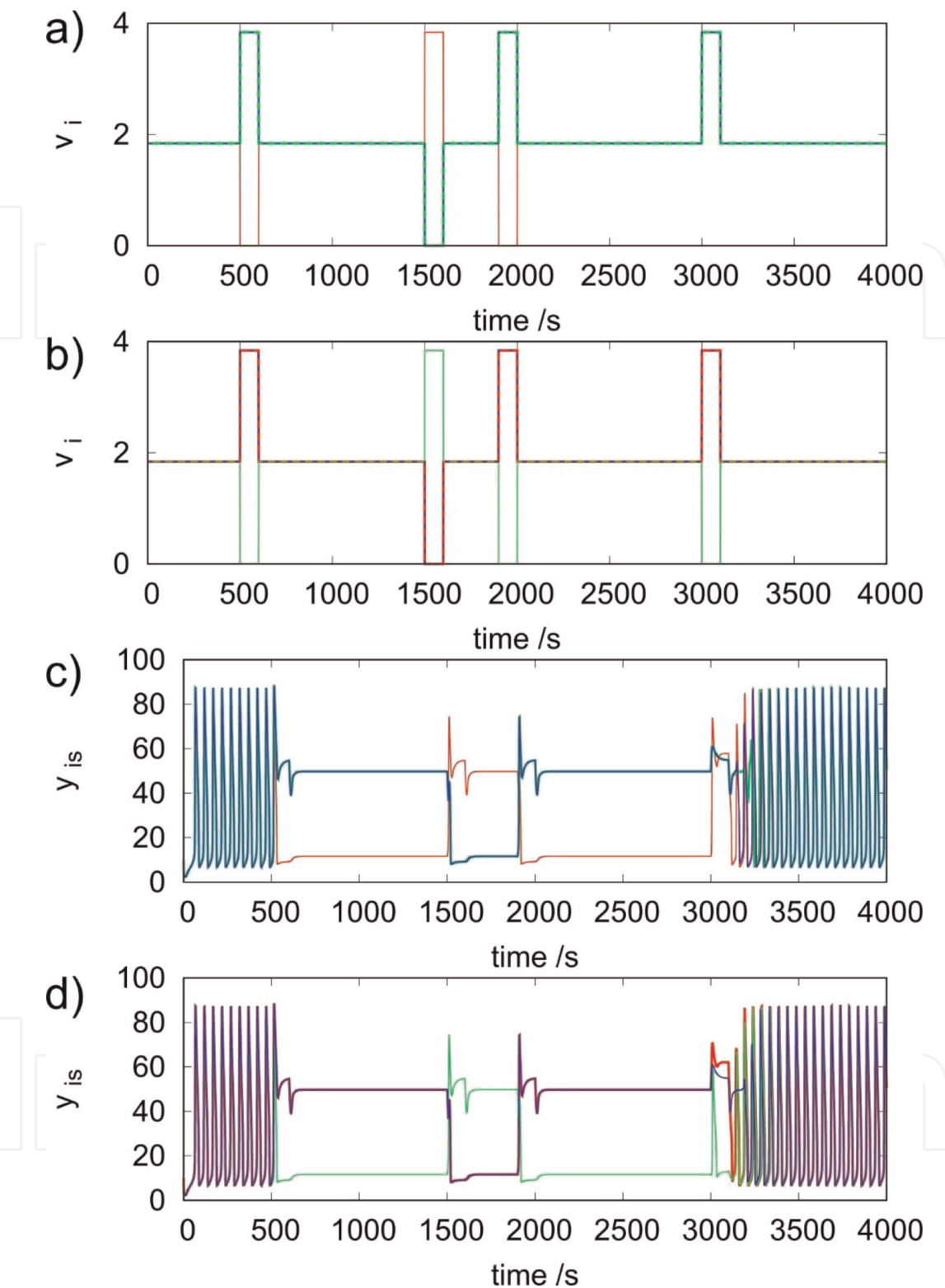


**Figure 3.** Dynamic simulation of transitions in between uniform oscillations and nonuniform discrete patterns,  $\sigma_M = 100 \text{ s}^{-1}$ ,  $\sigma_{inh} = 35 \text{ s}^{-1}$ ,  $k_d = 0.1 \text{ s}^{-1}$ : a) red curve represents  $v_1$ , the green curve represents  $v_{11}$ , the blue dashed curve represents  $v_6$ ; b) red curve represents  $v_2$ , the green curve represents  $v_{20}$ , and the blue dashed curve represents  $v_{10}$ ; c) ADP concentrations in selected cells: Red curve – Cell #1, green curve – Cell #11, blue curve – Cell #6 d) ADP concentrations in selected cells: Red curve – Cell #2, green curve – Cell #20, blue curve – Cell #10.

dependent concentration of ADP at cell 1, cell 6, and cell 11. **Figure 3d)** shows the concentration of ADP in cell 2, cell 10, and cell 20. The initial concentrations of both ATP and ADP in every cell are set at value 10, which leads to uniform oscillations. The

system oscillates until the first perturbation is applied at 500 seconds. We have decided to use only two types of perturbation values, and that is  $\nu_i(t) = 3.84 \text{ s}^{-1}$  and no flow of substrate,  $\nu_i(t) = 0 \text{ s}^{-1}$ , while outside perturbation times, the flow of substrate is set according to our previous studies as  $\nu_i(t) = 1.84 \text{ s}^{-1}$  [25]. The first perturbation is  $\nu_i(t_k) = 3.84 \text{ s}^{-1}$  for  $i = \{2,3,6,7,10,11,14,15,18,19\}$  and  $\nu_j(t_k) = 0 \text{ s}^{-1}$  for  $j = \{1,4,5,8,9,12,13,16,17,20\}$  applied in the time interval [500 s, 600 s]. It leads to a transition from uniform oscillation to nonuniform pattern type  $AE^2A^2E^2A^2E^2A^2E^2A$ . The second perturbation:  $\nu_i(t_l) = 0 \text{ s}^{-1}$  for  $i = \{2,3,6,7,10,11,14,15,18,19\}$  and  $\nu_j(t_l) = 3.84 \text{ s}^{-1}$  for  $j = \{1,4,5,8,9,12,13,16,17,20\}$  is applied in the time interval [1500s, 1600s]. This perturbation leads to a transition between two nonuniform patterns from type  $AE^2A^2E^2A^2E^2A^2E^2A$  to a type  $EA^2E^2A^2E^2A^2E^2A^2E$ . The third perturbation has the same  $\nu_i(t)$  values as the first perturbation, and it is applied in the time interval [1900s, 2000s]. It leads to a transition between two nonuniform stationary patterns from the type  $EA^2E^2A^2E^2A^2E^2A^2E$  to the type  $AE^2A^2E^2A^2E^2A^2E^2A$ . All the patterns in this example are the same type, just rotated by two cells toward each other. The fourth perturbation is defined as  $\nu_i(t_z) = 3.84 \text{ s}^{-1}$  for  $i = \{1,2,3,6,7,10,11,14,15,18,19\}$  and  $\nu_j(t_z) = 0 \text{ s}^{-1}$  for  $j = \{4,5,8,9,12,13,16,17,20\}$ , and it is applied in the time interval [3000 s, 3100 s]. The symmetry of  $\nu_i(t)$  values are selected such that they do not correspond to any stationary pattern for this parameter region. The application of such perturbation leads to a transition from pattern type  $AE^2A^2E^2A^2E^2A^2E^2A$  back to uniform oscillation. The uniform oscillations prevail until the end of the simulation at 4000 seconds.

To assess all accessible discrete nonuniform patterns, we used initial conditions taken from the solution diagram in **Figure 2**, or in case any pattern occurs for different parameters than those used in **Figure 2**, we took the initial conditions from the whole parameter space we have analyzed.

The first set of discrete nonuniform patterns is presented in **Figure 4**. The patterns in **Figure 4a** and **b**) show concentration profile  $E^2A^3E^2A^3E^2A^3E^2A^3$ . They occur for  $\sigma_{inh} = 60 \text{ s}^{-1}$  and  $k_d = 0.1 \text{ s}^{-1}$ . We can also describe the pattern using *wavenumber*, defined as the number of wavelengths per the distance of 20 cells. For the case of **Figure 4a** and **b**), the wavenumber is 4 for pattern  $E^2A^3$ . The patterns in **Figure 4c** and **d**) are different as they represent  $C^4DC^4DC^4DC^4D$  with wavenumber 4. They exist for  $\sigma_{inh} = 26 \text{ s}^{-1}$ ,  $k_d = 0.1 \text{ s}^{-1}$ . The nonuniform pattern in **Figure 4e**) has pattern  $A^2BCD^4CBA^2BCD^4CB$ , and it occurs for  $\sigma_{inh} = 35 \text{ s}^{-1}$ ,  $k_d = 0.55 \text{ s}^{-1}$ . The wavenumber of it is 2. This pattern is present in five rotations positions within the 2D blastula model. The remaining five rotation positions of this pattern are found for  $\sigma_{inh} = 60 \text{ s}^{-1}$  and  $k_d = 0.55 \text{ s}^{-1}$ , but we decided not to show it as the pattern  $A^2BCD^4CBA^2BCD^4CB$  is the same.

The second set of discrete nonuniform patterns is specific. **Figure 5** shows nine discrete patterns which coexist simultaneously for  $\sigma_{inh} = 35 \text{ s}^{-1}$  and  $k_d = 0.1 \text{ s}^{-1}$  and are not all just rotations of the same pattern. The patterns in **Figure 5a–d**) show concentration profile  $A^2E^2A^2E^2A^2E^2A^2E^2$ , which has wavenumber 5. The patterns in **Figure 5e–g**) appear to be somehow connected by their concentration profile values, but after careful examination, they are three different patterns. The pattern in **Figure 5e**) has the concentration code  $D^2CAD^2ACD^2A^2E^2A^2E^2A^2$ , the pattern in **Figure 5f**) has the concentration code  $DEA^2E^2A^2EDACDEA^2EDCA$ , and the **Figure 5g**) has the concentration code  $D^3A^2E^2A^2D^3ADEA^2EDA$ . The wavenumber of all three patterns is 1. These three patterns are highly irregular compared to other patterns, and they may be responsible for either unwanted development mutation or



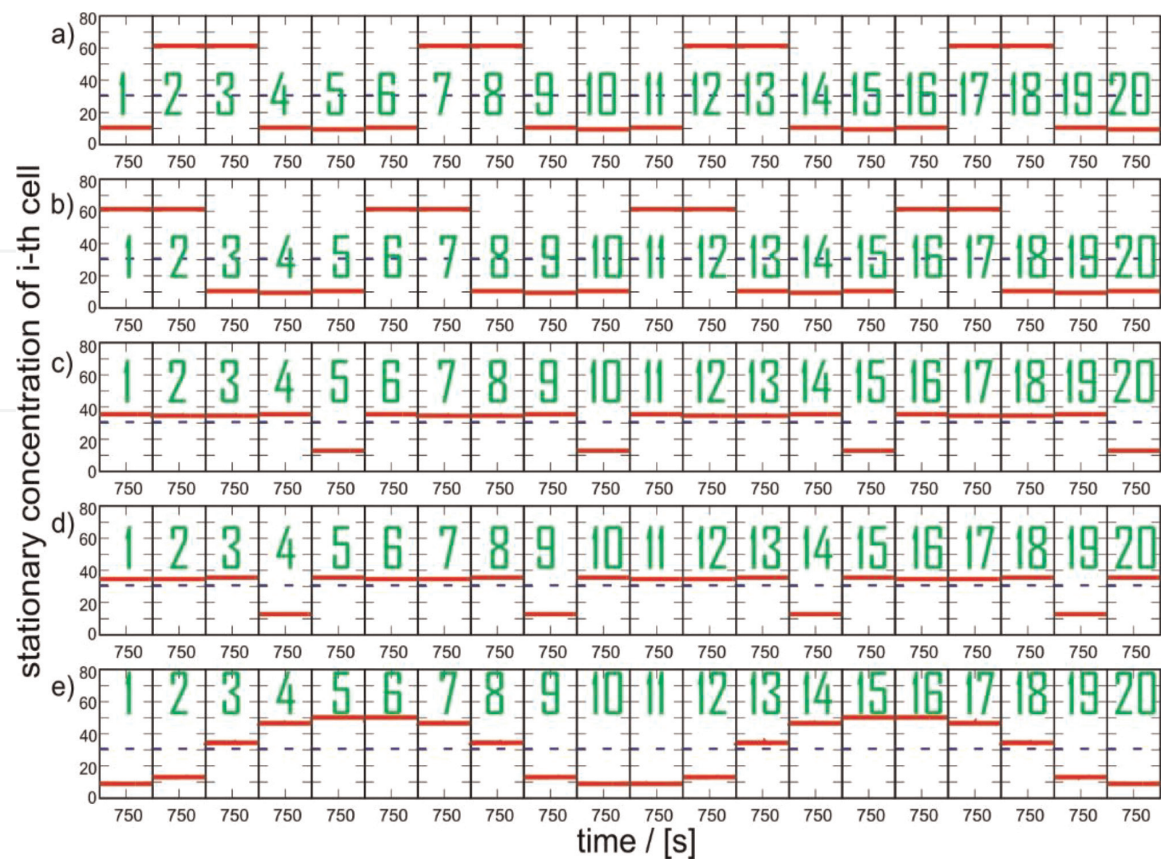


**Figure 4.** Discrete patterns of the stationary concentrations of ADP in 20 cells of the artificial blastula arranged in the time interval  $[500\text{ s}, 1000\text{ s}]$  for various sets of parameters  $\sigma_M = 100\text{ s}^{-1}$ . a)  $\sigma_{inh} = 60\text{ s}^{-1}$ ,  $k_d = 0.1\text{ s}^{-1}$ , b)  $\sigma_{inh} = 60\text{ s}^{-1}$ ,  $k_d = 0.1\text{ s}^{-1}$ , c)  $\sigma_{inh} = 26\text{ s}^{-1}$ ,  $k_d = 0.1\text{ s}^{-1}$ , d)  $\sigma_{inh} = 26\text{ s}^{-1}$ ,  $k_d = 0.1\text{ s}^{-1}$ , and e)  $\sigma_{inh} = 35\text{ s}^{-1}$ ,  $k_d = 0.55\text{ s}^{-1}$ . Each cell is numbered by a green number. The blue dashed line corresponds to ADP concentration in an unstable uniform stationary state. The red lines represent stationary concentrations of ADP in each cell.

are necessary to create some type of polarity in the organism for development beyond blastula and gastrula. The pattern in **Figure 5h** and **i**) has concentration profile  $A^2D^3A^2D^3A^2D^3A^2D^3$  and the wavenumber 4.

## 4. Discussion

The coexistence of multiple patterns for the same set of parameters illustrated in **Figure 5** allows for multiple morphogenetic results. Our analysis of the model has shown there is not a simple pattern with one minimum of concentration of ADP and one maximum of concentration of ADP, and with the wavenumber 1, which we would expect to start gastrulation. There are, however, three patterns with wavenumber 1, where we can observe certain concentration profiles with both maxima and minima.

This might be the pattern, which could start gastrulation as a result of a concentration profile in 10 cells altogether or all 20 cells. In these cases, we expect the gastrulation to start at  $D^2$  in between  $\dots CAD^2AC \dots$  or it can start at  $A^2$  in between  $\dots DEA^2ED \dots$  or finally it can occur at  $A^2$  in between  $\dots DEA^2ED \dots$ . We can notice the last two cases have the same structure. This might be either a mechanism to ensure that two patterns can lead to gastrulation or our universal 2D blastula model incorporating both gastrulation and limb development to multiple organisms with a tail and without a tail. Such organism would have only one axis of body symmetry. The

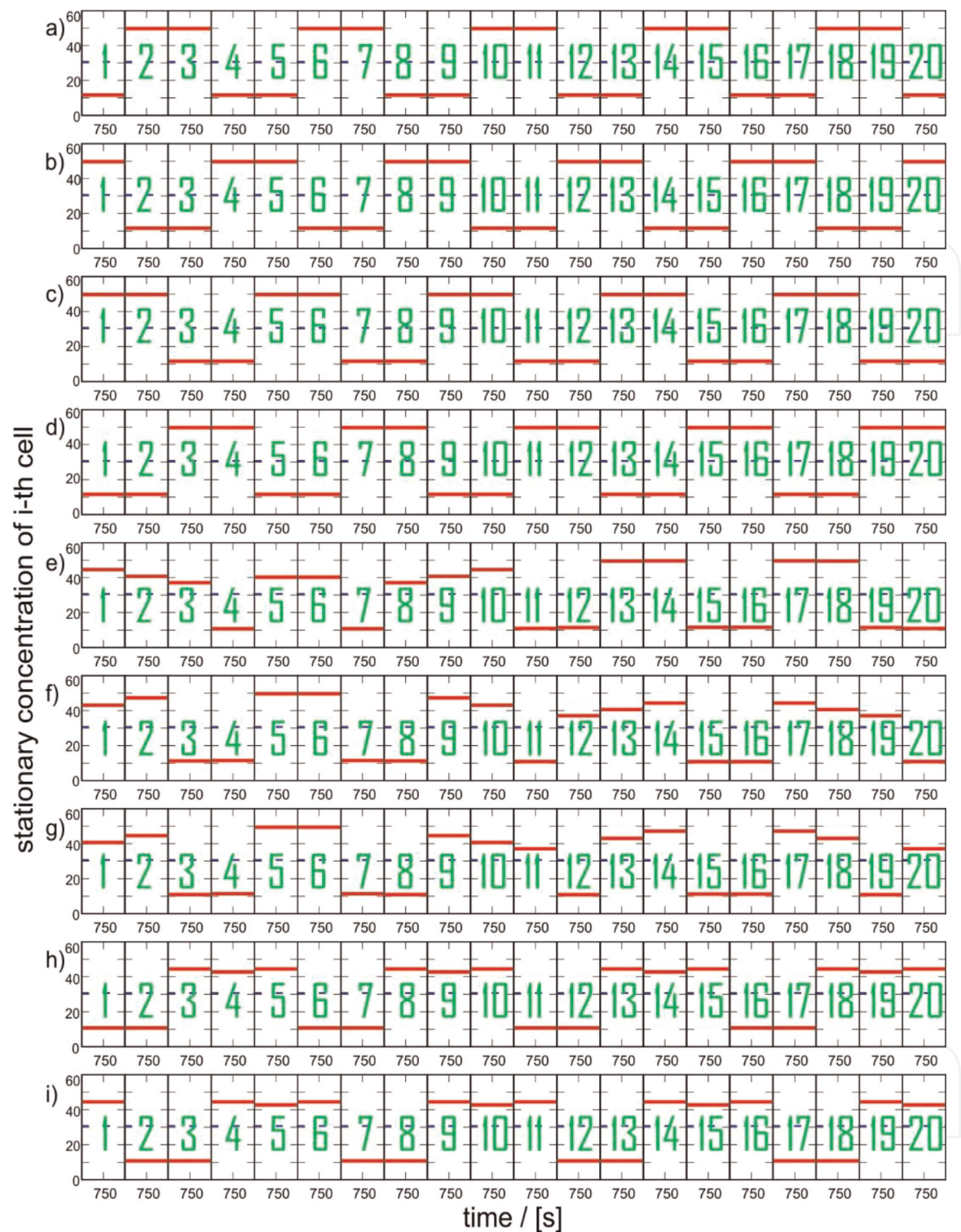


**Figure 5.**  
*Discrete patterns of the stationary concentrations of ADP in 20 cells of the artificial blastula arranged in the time interval [500 s, 1000 s] for  $\sigma_M = 100 \text{ s}^{-1}$ ,  $\sigma_{inh} = 35 \text{ s}^{-1}$ ,  $k_d = 0.1 \text{ s}^{-1}$  each cell is numbered by a green number. Notation is shown in Figure 4.*

concentration profiles show that a variety of perturbations can lead to the same pattern type, just rotated by a few cells. Since our model can also serve as a model for developing organism or may set prepatterns for future limb development creating multiple axes of body symmetry. The importance of growing legs on a position shifted by  $\pi/10$ , while all limbs have a constant position to each other, is insignificant. What



could be a problem if the perturbation switches the pattern from wavenumber 4 to wavenumber 5 or vice versa. A chemical causing this is toxic toward morphogenetic development, because the organism will grow a tail when it is not supposed to or vice versa. If applied to a growing palm, a perturbing chemical will influence a number of digits.

For the purpose of a method of obtaining chemoinformatics toxicity information in living developing organisms, our 2D blastula model serves only as a skeleton hybrid/artificial organism since it only works with ATP and ADP and takes into account only the anaerobic part of glycolysis via kinetic parameters. For the purpose of modeling the pattern behavior of cancer cells [49] due to the Warburg effect [50], it can be extended toward the full model of anaerobic glycolysis using the model proposed by Hynne et al. [51, 52]. If we want to assess the pattern toxicity toward cells with a whole glycolytic reaction chain, including aerobic part of glycolysis [7], it is possible to incorporate artificial mitochondria [53, 54].

Our long-term goal is the creation of an array [55] of artificial cells [56], which could simulate behavior of blastula or even start a shape development, depending on the capabilities of the artificial cell.

## 5. Conclusions

We have performed an analysis of the stability and bifurcation of stationary states for the 2D model of blastula consisting of 20 coupled cells. The chemistry of each cell is described by the two-variable model of glycolysis (cf. Eq. (3)). The system shows a remarkable number of discrete Turing patterns and can be used to model different phenomena.

One of them is the application of coupled cells as a chemical memory unit. Different patterns can be used for different symbol coding. **Figure 2** suggests a straightforward method of switching between discrete patterns. In order to optimize memory, an extensive study on the best strategy for switching between patterns is necessary.

The introduced model can also serve as an artificial living organism for studies on developmental toxicity. We have chosen a parameter plane of  $\sigma_{inh}$  or  $k_d$  while having constant  $\sigma_M = 100 \text{ s}^{-1}$ . Using dynamic simulation in program CONT by varying input function  $\nu_i(t) \in [0 \text{ s}^{-1}, 4 \text{ s}^{-1}]$  for each and every  $i$ -th cell for time 100 seconds, we have found and classified eight discrete patterns. Each pattern has been classified based on its concentration value by the letters ABCDE. We have found five patterns, which are just rotated within the 2D blastula and therefore can serve for future development or limbs as a prepattern, specifically  $E^2A^3$  with wavenumber 4,  $C^4D$  with wavenumber 4,  $A^2BCD^4CB$  with wavenumber 2,  $A^2E^2$  with wavenumber 5, and  $A^2D^3$  with wavenumber 4. These patterns can lead either to the organism growing four limbs or five limbs or growing four or five fingers on the limb. We have also found three patterns, which resent a discrete “wave” [cf. **Figure 5e–g**]. However, these patterns have mirror symmetry and therefore cannot have wavenumber 2. It opens an opportunity for gastrulation, or it can lead to a prepattern for later body symmetry development with one axis. These patterns are specifically  $D^2CAD^2ACD^2A^2E^2A^2E^2A^2$ ;  $DEA^2E^2A^2EDACDEA^2EDCA$ , and  $D^3A^2E^2A^2D^3ADEA^2EDA$ . In these cases, we expect the gastrulation to start at  $D^2$  in between ...  $CAD^2AC$  ... or it can start at  $A^2$  in between ...  $DEA^2ED$  ... or finally it can occur at  $A^2$  in between ...  $DEA^2ED$  ...

Our analysis of pattern occurrence inside artificial 2D blastula should generalize the current cheminformatics methods to include toxicological databases toward the

potential development of living organisms while not actually harming animals. It can also extend cheminformatics databases about toxicity toward cancer cells, since the model incorporates anaerobic glycolysis and, therefore, can describe the Warburg effect. The model currently works with ATP and ADP but can be extended toward all species taking part in glycolysis. It can also incorporate artificial mitochondria to work with aerobic glycolysis.

## Acknowledgements

This publication is part of a project that has received funding from the European Union's Horizon 2020 research and innovation program under the Marie Skłodowska-Curie grant agreement No. 847413.

Scientific work published as part of an international co-financed project founded from the program of the Minister of Science and Higher Education entitled "PMW" in the years 2020–2024; agreement no. 5005/H2020-MSCA-COFUND/2019/2.

## Conflict of interest

"The authors declare no conflict of interest."

## Data availability


All numerical data and the model are stored in the repository at: <https://doi.org/10.18150/JKFBW>

## Author details

František Muzika\* and Jerzy Górecki  
Institute of Physical Chemistry Polish Academy of Sciences, Warsaw, Poland

\*Address all correspondence to: [fmuzika@ichf.edu.pl](mailto:fmuzika@ichf.edu.pl)

## IntechOpen

© 2023 The Author(s). Licensee IntechOpen. This chapter is distributed under the terms of the Creative Commons Attribution License (<http://creativecommons.org/licenses/by/3.0>), which permits unrestricted use, distribution, and reproduction in any medium, provided the original work is properly cited. 



## References

- [1] Tongman S, Chanama S, Chanama M, Plaimas K, Lursinsap C. Metabolic pathway synthesis based on predicting compound transformable pairs by using neural classifiers with imbalanced data handling. *Expert Systems with Applications*. 2017;**88**:45-57. DOI: 10.1016/j.eswa.2017.06.026
- [2] Medina-Franco JL, Thomas Caulfield T. Advances in the computational development of DNA methyltransferase inhibitors. *Drug Discovery Today*. 2011;**16**:418-425. DOI: 10.1016/j.drudis.2011.02.003
- [3] Enoch SJ, Hasarova Z, Cronin MTD, Bridgwood K, Rao S, Kluxen FM, et al. Sub-structure-based category formation for the prioritisation of genotoxicity hazard assessment for pesticide residues: Sulphonyl ureas. *Regulatory Toxicology and Pharmacology*. 2022;**129**:105115. DOI: 10.1016/j.yrtph.2022.105115
- [4] Rizvi NF, Santa Maria JP, Nahvi A, Klappenbach J, Klein DJ, Curran PJ, et al. Targeting RNA with small molecules: Identification of selective, RNA-binding small molecules occupying drug-like chemical space. *SLAS Discovery*. 2020;**25**:384-396. DOI: 10.1177/2472555219885373
- [5] Manigrasso J, Marcia M, De Vivo M. Computer-aided design of RNA-targeted small molecules: A growing need in drug discovery. *Chem*. 2021;**7**:2965-2988. DOI: 10.1016/j.chempr.2021.05.021
- [6] Ansari MHR, Saher S, Parveen R, Khan W, Khan IA, Ahmad S. Role of gut microbiota metabolism and biotransformation on dietary natural products to human health implications with special reference to biochemoinformatics approach. *Journal of Traditional and Complementary Medicine*. 2022. DOI: 10.1016/j.jtcme.2022.03.005 [In press]
- [7] Wills LP. The use of high-throughput screening techniques to evaluate mitochondrial toxicity. *Toxicology*. 2017;**391**:34-41. DOI: 10.1016/j.tox.2017.07.020
- [8] Lo YC, Senese S, France B, Gholkar AA, Damoiseaux R, Torres JZ. Computational cell cycle profiling of Cancer cells for prioritizing FDA-approved drugs with repurposing potential. *Scientific Reports*. 2017;**7**:2045-2322. DOI: 10.1038/s41598-017-11508-2
- [9] Amo del EM, Rimpelä AK, Heikkinen E, Kari OK, Ramsay E, Lajunen T, et al. Pharmacokinetic aspects of retinal drug delivery. *Progress in Retinal and Eye Research*. 2017;**57**:134-185. DOI: 10.1016/j.preteyeres.2016.12.001
- [10] Flores-Carrillo P, Velázquez-López JM, Aguayo-Ortiz R, Hernández-Campos A, Trejo-Soto PJ, Yépez-Mulia L, et al. Synthesis, antiprotozoal activity, and chemoinformatic analysis of 2-(methylthio)-1H-benzimidazole-5-carboxamide derivatives: Identification of new selective giardicidal and trichomonocidal compounds. *European Journal of Medicinal Chemistry*. 2017;**137**:211-220. DOI: 10.1016/j.ejmech.2017.05.058
- [11] Ghiano DG, Recio-Balsells A, Bortolotti A, Defelipe LA, Turjanski A, Morbidoni HR, et al. New one-pot synthesis of anti-tuberculosis compounds inspired on isoniazid. *European Journal of Medicinal Chemistry*. 2020;**208**:112699. DOI: 10.1016/j.ejmech.2020.112699

- [12] Gajewicz-Skretna A, Gromelski M, Wyrzykowska E, Furuham A, Yamamoto H, Suzuki N. Aquatic toxicity (Pre)screening strategy for structurally diverse chemicals: Global or local classification tree models? *Ecotoxicology and Environmental Safety*. 2021;**208**: 111738. DOI: 10.1016/j.ecoenv.2020.111738
- [13] Chan HCS, Shan H, Dahoun T, Vogel H, Yuan S. Advancing drug discovery via artificial intelligence. *Trends in Pharmacological Sciences*. 2019;**40**:592-604. DOI: 10.1016/j.tips.2019.06.004
- [14] Sansare S, Duran T, Mohammadiarani H, Goyal M, Yenduri G, Costa A, et al. Artificial neural networks in tandem with molecular descriptors as predictive tools for continuous liposome manufacturing. *International Journal of Pharmaceutics*. 2021;**603**:120713. DOI: 10.1016/j.ijpharm.2021.120713
- [15] Cai D, van Rijsbergen CJ. Learning semantic relatedness from term discrimination information. *Expert Systems with Applications*. 2009;**36**: 1860-1875. DOI: 10.1016/j.eswa.2007.12.072
- [16] Turing A. The chemical basis of morphogenesis. *Philosophical Transactions on Royal Society London B*. 1952;**237**:37-72. DOI: 10.1098/rstb.1952.0012
- [17] Kozubowski L, Saito K, Johnson JM, Howell AS, Zyla TR, Lew DJ. Symmetry-breaking polarization driven by a Cdc42p GEF-PAK complex. *Current Biology*. 2008;**18**:1719-1726. DOI: 10.1016/j.cub.2008.09.060
- [18] Castro-e-Silva A, Bernardes AT. Gastrulation as a self-organized symmetry breaking process. *Physica A: Statistical Mechanics and its Applications*. 2005;**352**:535-546. DOI: 10.1016/j.physa.2004.10.039
- [19] Murray JD. *Mathematical Biology II: Spatial Models and Biomedical Applications*. Third ed. USA: Springer Science+Business, Media, LLC; 2003. DOI: 10.1007/b98869
- [20] Bagudu A, Kraemer C, Germann P, Menshykau D, Iber D. Digit patterning during limb development as a result of the BMP-receptor interaction. *Scientific Reports*. 2012;**991**:1-13. DOI: 10.1038/srep00991
- [21] Meinhardt M, Gierer A. Application of a theory of biological pattern formation based on lateral inhibition. *Journal of Cell Science*. 1974;**15**:321-346
- [22] Meinhardt M, Gierer A. Pattern formation by local self-activation and lateral inhibition. *BioEssays*. 2000;**22**: 753-760. DOI: 10.1002/1521-1878(200008)22:8<753::AID-BIES9>3.0.CO;2-Z
- [23] Vastano JA, Pearson JE, Horsthemke W, Swinney HL. Chemical pattern formation with equal diffusion coefficients. *Physics Letters A*. 1987;**124**: 320-324. DOI: 10.1016/0375-9601(87)90019-3
- [24] Vastano JA, Pearson JE, Horsthemke W, Swinney LH. Turing patterns in an open reactor. *The Journal of Chemical Physics*. 1988;**88**:6175-6181. DOI: 10.1063/1.454456
- [25] Muzika F, Schreiber I. Control of Turing patterns and their usage as sensors, memory arrays, and logic gates. *The Journal of Chemical Physics*. 2013;**139**:164108. DOI: 10.1063/1.4825379
- [26] Muzika F, Schreiberová L, Schreiber I. Discrete Turing patterns in

coupled reaction cells in a cyclic array. *Reaction Kinetic Mechanism Catalysis*. 2016;**118**:99-114. DOI: 10.1007/s11144-016-1004-y

[27] Asakura K, Konishi R, Nakatani T, Nakano T, Kamata M. Turing pattern formation by the CIMA reaction in a chemical system consisting of quaternary alkyl ammonium cationic groups. *The Journal of Physical Chemistry. B*. 2011;**115**:3959-3963. DOI: 10.1021/jp111584u

[28] Horváth J, Szalai I, De Kepper P. Designing stationary reaction–diffusion patterns in pH self-activated systems. *Accounts of Chemical Research*. 2018; **51**(12):3183-3190. DOI: 10.1021/acs.accounts.8b00441

[29] Castets V, Dulos E, Boissonade J, Kepper PD. Experimental evidence of a sustained standing Turing-type nonequilibrium chemical pattern. *Physical Review Letters*. 1990;**64**: 2953-2956. DOI: 10.1103/PhysRevLett.64.2953

[30] Rudovics B, Barillot E, Davies PW, Dulos E, Boissonade J, Kepper PD. Experimental studies and quantitative Modeling of Turing patterns in the (chlorine dioxide, iodine, malonic acid) reaction. *The Journal of Physical Chemistry. A*. 1999;**103**:1790-1800. DOI: 10.1021/jp983210v

[31] Sanz-Anchelergues A, Zhabotinsky AM, Epstein IR, Muñuzuri AP. Turing pattern formation induced by spatially correlated noise. *Physical Review E*. 2001;**63**:056124. DOI: 10.1103/PhysRevE.63.056124

[32] Berenstein IB, Dolník M, Yang L, Zhabotinsky AM, Epstein IR. Turing pattern formation in a two-layer system: Superposition and superlattice patterns. *Physical Review E*. 2004;**70**:046219. DOI: 10.1103/PhysRevE.70.046219

[33] Bar-Eli K. Coupling of chemical oscillators. *The Journal of Physical Chemistry*. 1984;**88**:3616-3622. DOI: 10.1021/j150660a048

[34] Bar-Eli K, Reuveni S. Stable stationary states of coupled chemical oscillators. Experimental evidence. *The Journal of Physical Chemistry*. 1985;**89**: 1329-1330. DOI: 10.1021/j100254a002

[35] Dolník M, Berenstein I, Zhabotinsky AM, Epstein IR. Spatial periodic forcing of Turing structures. *Physical Review Letters*. 2001;**87**:238301. DOI: 10.1103/PhysRevLett.87.238301

[36] Dolník M, Marek M. Extinction of oscillations in forced and coupled reaction cells. *The Journal of Physical Chemistry*. 1988;**92**:2452-2455. DOI: 10.1021/j100320a014

[37] Crowley MF, Epstein IR. Experimental and theoretical studies of a coupled chemical oscillator: Phase death, multistability, and in-phase and out-of-phase entrainment. *The Journal of Physical Chemistry*. 1989;**93**:2496-2502. DOI: 10.1021/j100343a052

[38] Yoshimoto M, Yoshikawa K, Mori Y. Coupling among three chemical oscillators: Synchronization, phase death, and frustration. *Physical Review E*. 1993;**47**:864-874. DOI: 10.1103/PhysRevE.47.864

[39] Muzika F, Valent I. Irregular oscillations and symmetry breaking in a ring of coupled cells with yeast extract. 2022; DOI: 10.18150/GB24WE

[40] Górecki J, Bose A. Computing with networks of chemical oscillators and its application for schizophrenia diagnosis. *Frontier in Chemical Science*. 2022;**10**:



848685. DOI: 10.3389/fchem.2022.848685

[41] Górecki J, Bose A. How does a simple network of chemical oscillators see the Japanese flag? *Frontiers in Chemistry*. 2020;**09**:580703. DOI: 10.3389/fchem.2020.580703

[42] Goldbeter A, Moran F. Onset of birhythmicity in a regulated biochemical system. *Biophysical Chemistry*. 1984;**20**: 149-156. DOI: 10.1016/0301-4622(84)80014-9

[43] Mair T, Warnke C, Tsuji K, Müller SC. Control of glycolytic oscillations by temperature. *Biophysical Journal*. 2005;**88**:639-646. DOI: 10.1529/biophysj.104.043398

[44] Hereng TH, Elgstøen KBP, Eide L, Rosendal KR, Skålhegg BS. Serum albumin and HCO<sub>3</sub><sup>-</sup> regulate separate pools of ATP in human spermatozoa. *Human Reproduction*. 2014;**29**:918-930. DOI: 10.1093/humrep/deu028

[45] Mediavilla D, Metón I, Baanate IV. Purification and kinetic properties of 6-phosphofructo-1-kinase from gilthead sea bream muscle. *Biochimica et Biophysica Acta*. 2007;**1770**:706-715. DOI: 10.1016/j.bbagen.2006.11.014

[46] Nazarea AD. Spatiotemporal pattern formation in thin layers and membranes: Critical focal size. *Proceedings of the National Academy Science*. 1974;**71**: 3751-3753. DOI: 10.1073/pnas.75.9.4313

[47] Kubiček M, Marek M. *Computational Methods In Bifurcation Theory and Dissipative Structures*. New York, NY: Springer Verlag; 1983. p. 243. DOI: 10.1007/978-3-642-85957-1

[48] Kohout M, Schreiber I, Marek M. A computational tool for nonlinear dynamical and bifurcation analysis of

chemical engineering problems. *Computer Chemical Engineering*. 2002; **26**:517-527. DOI: 10.1016/S0098-1354(01)00783-9

[49] Feng L, Reynisdóttir I, Reynisson J. The effect of PLC- $\gamma$ 2 inhibitors on the growth of human tumour cells. *European Journal of Medicinal Chemistry*. 2012;**54**:463-469. DOI: 10.1016/j.ejmech.2012.05.029

[50] Warburg O. On the origin of cancer cells. *Science*. 1956;**123**(3191):309-314. DOI: 10.1126/science.123.3191.309

[51] Hynne F, Danø S, Sørensen PG. Full-scale model of glycolysis in *Saccharomyces cerevisiae*. *Biophysical Chemistry*. 2001;**94**:121-163. DOI: 10.1016/S0301-4622(01)00229-0

[52] Herdeen van JH, Wortel MT, Bruggeman FJ, Heijnen JJ, Bollen YJM, Planqué R, et al. Lost in transition: Start-up of glycolysis yields subpopulations of nongrowing cells. *Science*. 2014;**343**: 1245114. DOI: 10.1126/science.1245114

[53] Kumar S, Karmacharya M, Michael IJ, Choi Y, Kim J, Kim IU, et al. Programmed exosome fusion for energy generation in living cells. *Nature Catalysis*. 2021;**4**:763-774. DOI: 10.1038/s41929-021-00669-z

[54] Thakur A, Johnson A, Jacobs E, Zhang K, Chen J, Wei Z, et al. Energy sources for exosome communication in a Cancer microenvironment. *Cancers*. 2022;**14**(7):1698. DOI: 10.3390/cancers14071698

[55] Li DY, Zhou ZH, Yu YL, Deng NN. Microfluidic construction of cytoskeleton-like hydrogel matrix for stabilizing artificial cells. *Chemical Engineering Science*. 2022;**264**:118186. DOI: 10.1016/j.ces.2022.118186



[56] Herianto S, Chien PJ, Ho JA, Tu HL.  
Liposome-based artificial cells: From  
gene expression to reconstitution of  
cellular functions and phenotypes.  
Biomaterials Advances. 2022;**142**:213156.  
DOI: 10.1016/j.bioadv.2022.213156

IntechOpen

IntechOpen